



Trans. Nonferrous Met. Soc. China 31(2021) 3439-3451

Transactions of Nonferrous Metals Society of China

www.tnmsc.cn



Oxidation and tribological properties of anodized Ti45Al8.5Nb alloy

Zhe-xuan LI¹, Ya-ting BAO², Lian-kui WU¹, Fa-he CAO¹

- 1. School of Materials, Shenzhen Campus of Sun Yat-sen University, Shenzhen 518107, China;
- 2. College of Materials Science and Engineering, Zhejiang University of Technology, Hangzhou 310014, China

Received 28 July 2021; accepted 2 November 2021

Abstract: The oxidation performance and tribological properties of the anodized Ti45Al8.5Nb were investigated. Anodization was performed in ethylene glycol containing 0.15 mol/L NH₄F. Results showed that the anodized Ti45Al8.5Nb alloy exhibited good resistance against oxidation. After 100 h oxidation at 1000 °C, the mass gain of the anodized Ti45Al8.5Nb alloy was only 0.37 mg/cm^2 . This is attributed to the generation of protective oxide scale. On the other hand, the hardness and elastic modulus of the anodized Ti45Al8.5Nb alloy decreased and then increased with the prolonging of thermal exposure due to the generation of the Al₂O₃-enriched outermost oxide layer.

Key words: titanium aluminum alloy; anodization; high temperature oxidation; tribological properties

1 Introduction

TiAl-based alloys are considered to be ideal lightweight high-temperature structural materials owing to their low density and excellent mechanical properties [1-5]. However, the inferior oxidation resistance above 800 °C restricts their potential application [6,7]. Over the past several decades, a great deal of effort has been devoted to enhancing the high temperature oxidation resistance of TiAl alloys via alloying design and surface modification. Alloying design, achieved by the addition of a third alloying element, such as Nb [8,9], B [10], Cr [11], Co [12], Y [13], and Si [14] is beneficial to increasing the proportion of Al₂O₃ in the oxide scale, therefore improving the oxidation performance. But excessive alloying elements will reduce the advantage of low density of TiAl alloys and deteriorate the mechanical properties [15]. Surface modification, including ion implantation [16,17], spraying fluorine containing polymer [18,19], applying a protective coating [20,21], and cathode plasma electrolysis [22–24] can efficiently improve the oxidation performance but has little influence on the mechanical properties of TiAl.

The tribological properties, such as elastic modulus, hardness, friction coefficient and wear behavior are other critical properties that even often limit the overall lifetime of components in industrial applications. RASTKAR et al [25] found that the shedding of lamellar grains caused by the friction stress was the main reason for the poor wear resistance of lamellar TiAl alloy. CHENG et al [26] and QIU et al [27] investigated the influence of service environment on the wear properties of TiAl alloy and found that the wear rate of TiAl alloy exposed in atmospheric was remarkably higher than that serviced in oxygen-free environment. The poor wear resistance of TiAl alloy in atmosphere was ascribed to the quick oxidation of Ti and Al. To enhance the wear resistance of TiAl alloys, surface treatment technologies such as laser treatment [28], micro-arc oxidation [29], and thermal oxidation treatment [30] have been employed. TIAN et al [31] pointed out that the changes in the tribological properties, as well as the oxidation performance, should be taken into comprehensive consideration when the alloy was served under elevated temperatures. However, less attention has been paid to the tribological properties of the alloys whose oxidation resistance has been improved by various strategies. XU et al [32] investigated the wear behavior of TiAl alloy with Al₂O₃/Al coating at 500 °C.

Recently, a novel strategy has been proposed to improve the oxidation resistance of TiAl alloys by anodization in an ethylene glycol/NH₄F solution system [33,34]. In these studies, fluoride ions were introduced to the surface of TiAl alloys by anodization. When exposed to high temperature in air, titanium fluorine would be volatilized and aluminum fluorine would be transferred into Al₂O₃, leading to the formation of a compact and protective Al₂O₃ layer and providing good oxidation resistance when exposed to air at the high temperatures [33,34]. Whereas, the effect of anodization on the tribological properties, such as the elastic modulus, hardness, friction coefficient and wear behavior of the TiAl alloy has not been investigated. These properties are highly dependent on the composition and structure of the oxide scale which are changed with the prolonging of oxidation time. In the present work, the oxidation performance and tribological properties of the anodized Ti45Al8.5Nb alloy were investigated.

2 Experimental

2.1 Anodization process of Ti45Al8.5Nb alloy

Ti45Al8.5Nb alloy (the alloy elements are shown in Table 1) was prepared using induction skull melting and remelted 12 times to reduce its composition heterogeneity. The homogenized ingot was cut into pieces of 15 mm × 15 mm × 2 mm by wire-electrode cutting (DK77120, Taizhou Zhongxing CNC Machine tool Factory, China) and ground by sandpaper with the grit of 300[#] (WAW7, Shanghai Shenming Abrasives Co., Ltd.) to remove the natural oxide scale, then ultrasonically cleaned in acetone and ethanol for 5 min sequentially, and finally rinsed with deionized water and dried with warm air. During the anodization process, two graphite plates (100 mm × 40 mm) were placed face to face with a distance of 5 cm, acting as the counter electrodes. The TiAl alloy was placed in the middle of the two graphite plates and acted as the working electrode. Anodization was carried out in ethylene glycol containing 0.15 mol/L NH₄F at 30 V and lasted for 1 h (DP3020, Mestek, China). During the anodization process, the electrolyte was magnetically stirred at 10 r/min and the reaction temperature was controlled at 25 °C. After anodization, the TiAl alloy was taken out from the electrolyte and ultrasonically cleaned in deionized water, acetone, and anhydrous ethanol sequentially, and finally dried by warm air.

Table 1 Alloy element contents (at.%)

Ti	Al	Nb	В	Y
46.26	45.00	8.50	0.02	0.02

2.2 Oxidation and characterization of anodized Ti45Al8.5Nb alloy

The oxidation behavior of the anodized Ti45Al8.5Nb alloy was investigated at 1000 °C in a box-type sintering furnace (KSL-1200X, Hefei Kejing Materials Technology Co., Ltd., China). Each specimen was perpendicularly put in a corundum crucible respectively and leaned on the inner wall of the crucible, and then put in the furnace with a temperature stabilized at 1000 °C. The specimens were removed from the furnace at select time intervals and cooled to room temperature in air for at least 60 min. The mass gain per exposed area (mg/cm²) was used to evaluate the oxidation resistance, which was achieved by an electronic balance with a sensitivity of 0.0001 g (BS124S, Sartorius, Germany). X-ray diffraction (Panalytical X'Pert PRO, Cu K_{α} (λ =0.154056 nm, 40 kV, 40 mA) was used to analyze the phase composition of the specimens. The microstructures composition of the specimens characterized by scanning electron microscopy (SEM, FEI nano nova 450) and an energy spectrometer (EDS, Oxford 80X). Three samples were used for each condition in the oxidation test.

2.3 Characterization of tribological properties of anodized Ti45Al8.5Nb alloy

Dry-sliding wear tests of the anodized Ti45Al8.5Nb alloy were carried out under atmospheric conditions at 298 K by a ball-on-disc tribometer (UMT-3, USA). The specimens were rotated by sliding against a stationary ball slider for 1800 s under a load of 5 N. Commercially available

Al₂O₃ balls with a diameter of 4 mm were used as the counterpart balls. Mean maximum wear depth was determined using contact profilometry (Dektak 150, Veeco, USA). Indentation experiments were carried out via the commercial nanoindentation tester (Micro Materials, Nano Test Vantage). The hardness and elastic modulus were calculated from the indentation experiment. The applied loads for the nanoindentation tests were all 16 mN with loading rates ranging from 0.05 to 2 mN/s and unloading 90% after holding for 5 s. In the measurement, the Poisson ratio was set as 0.25 and the maximum indentation depth was kept at 20% of the coating thickness (~500 nm) to minimize substrate effects. For each condition, one sample was employed during the mechanical properties test.

3 Results and discussion

3.1 Oxidation behavior

Figure 1 shows the oxidation kinetic curves of bare and anodized Ti45Al8.5Nb alloys during exposure to air at 1000 °C. After oxidation for 100 h, the bare Ti45Al8.5Nb alloy was seriously oxidized and the mass gain is as high as ~4.06 mg/cm². In contrast, the mass gain of the anodized Ti45Al8.5Nb is dramatically reduced to 0.37 mg/cm². Moreover, during the oxidation process, severe scale spallation was found on bare Ti45Al8.5Nb alloy, resulting in the exposure of the fresh substrate and further oxidation. As revealed in the optical image (the upper right corner), only a small portion of the bare Ti45Al8.5Nb alloy is covered by loose oxide scale and most of the

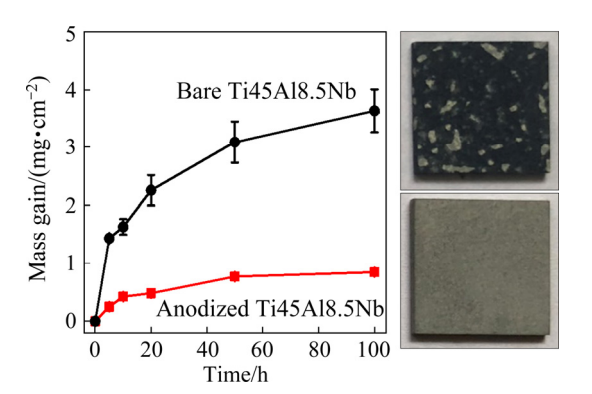


Fig. 1 Oxidation kinetic curves of bare (a) and anodized (b) Ti45Al8.5Nb alloys during exposure to air at 1000 °C (The insets are the optical images of the specimens after oxidation for 100 h)

outmost layer of the oxide scale spalls off from the substrate during the thermal exposure. Whereas, no obvious oxidation is observed on the anodized Ti45Al8.5Nb alloy and no scale spallation is found during the whole oxidation test (the bottom right corner), suggesting the remarkably improved oxidation resistance and anti-spallation performance of the oxide scale.

This phenomenon is ascribed to the halogen effect, which will result in the formation of a compact and protective Al₂O₃ scale [16,34]. In detail, during the anodization process, aluminum fluoride and titanium fluoride will generate on the surface of Ti45Al8.5Nb. During thermal exposure, titanium fluoride will evaporate when the temperature is higher than 300 °C [35]. At the same time, aluminum fluoride turns to be gaseous and outward migration through the cracks and pores of the initial oxide scale. With the increase of oxygen partial pressure near the surface of the oxide scale, the aluminum fluoride is oxidized to the protective and continuous Al₂O₃ scale.

3.2 Surface morphology and composition

Figure 2 shows the top-surface SEM images of bare and anodized Ti45Al8.5Nb alloys. displayed in Figs. 2(a) and (b), the bare Ti45Al8.5Nb alloy is flat except for some abrasion scratches generated during the surface grinding process. Whereas, the anodized Ti45Al8.5Nb alloy is full of small holes and micro-cracks (Figs. 2(c) and (d)), which are formed due to the anodization in NH₄F-containing electrolyte. The EDS analysis indicates that the anodic film is Al- and Fenriched (Table 2). Notably, the morphology of anodized TiAl alloy is highly dependent on the composition of alloy and anodization parameters, such as anodization voltage and electrolyte composition [33,34,36,37]. Generally, the low anodization voltage and low fluorine concentration result in the formation of a compact and thin anodic film, while the porous and thick anodic film will be generated under high anodization voltage and high fluorine concentration [34]. Previous results indicate that the oxidation performance of the specimen with compact and thin anodic film deteriorates after oxidation at 1000 °C for 500 h, but the specimen with porous and thick anodic film could provide good oxidation resistance for 1000 h.

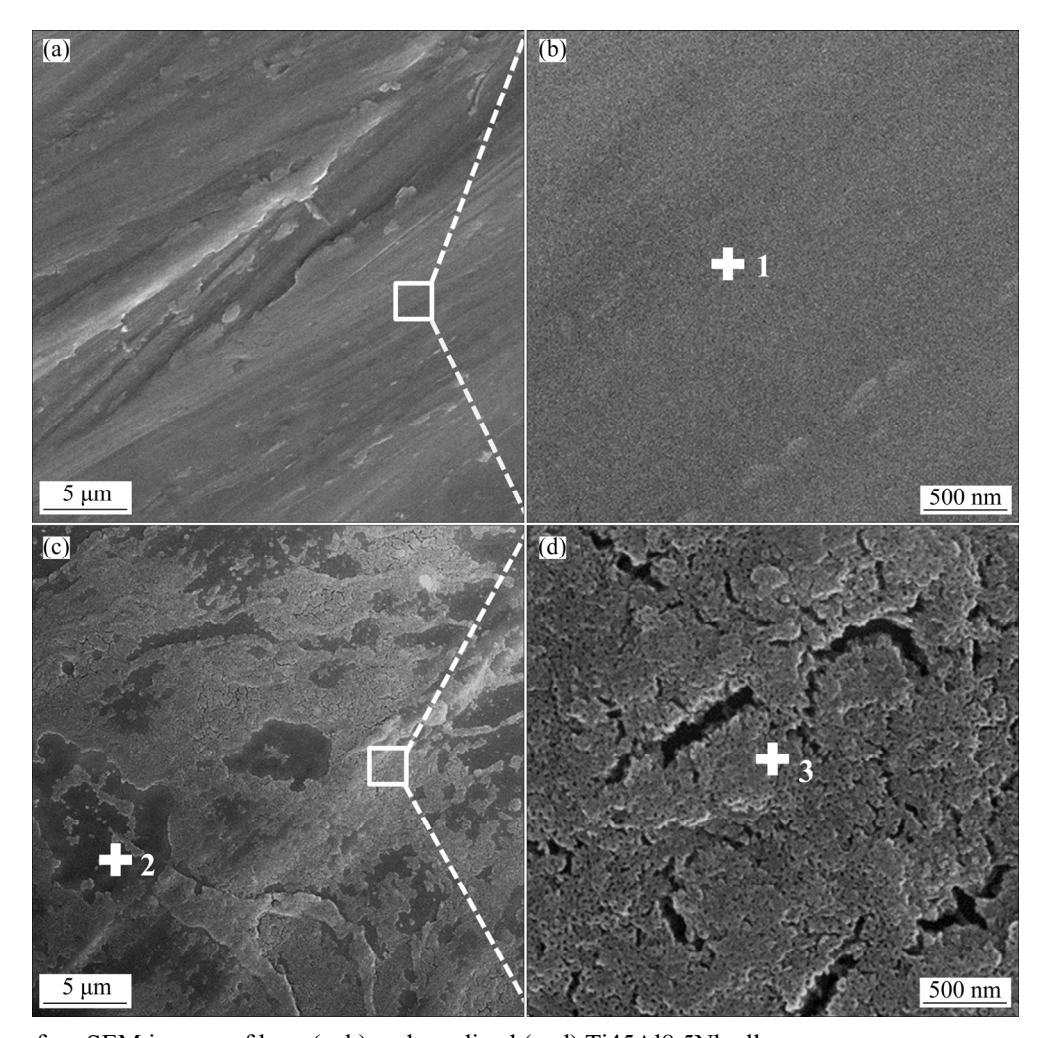


Fig. 2 Top-surface SEM images of bare (a, b) and anodized (c, d) Ti45Al8.5Nb alloys

Table 2 Chemical compositions of positions marked in Fig. 2

Position	Composition/at.%				
	Ti	Al	Nb	O	F
1	42.24	41.01	6.96	9.79	_
2	32.14	31.42	5.38	23.21	7.85
3	41.21	39.24	7.13	10.63	1.79

When exposed to air at 1000 °C, the evolution of the surface morphology and chemical composition of the anodized Ti45Al8.5Nb alloy was recorded by SEM and EDS, respectively. As revealed in Fig. 3, with the prolonging of oxidation time, the top surface of the specimens gradually turns to be compact and rough. After oxidation for 1 h, a porous oxide scale composed of many segregated particles is found on the specimen (Figs. 3(a) and (b)). This is attributed to the volume shrinkage caused by the formation and growth of

Al₂O₃ and TiO₂ from the anodic film. At the same time, the EDS analysis reveals that no fluorine can be detected on the specimen anymore (see Point 1 in Fig. 3(b) and Table 3). This can be ascribed to the evaporation of the titanium fluoride and the transformation of aluminum fluoride into Al₂O₃ [33,34]. When the oxidation time is beyond 5 h (Figs. 3(e)-(1)), the holes and cracks observed in the pristine anodized specimen (Figs. 2(c) and (d)) gradually disappear and ravine-like morphology emerges. Additionally, the scales on all specimens are composed of aluminum- and titanium-based oxide particles whose sizes increase with the prolonging of oxidation time. Notably, the O content gradually increases with the prolonging of oxidation time, while the Al and Ti contents reduce correspondingly (see Points 2-6 in Figs. 3(d-1) and Table 3). Interestingly, the Al content is much higher than the Ti content in all specimens and the mole ratio of Al to Ti in the oxide scale gradually

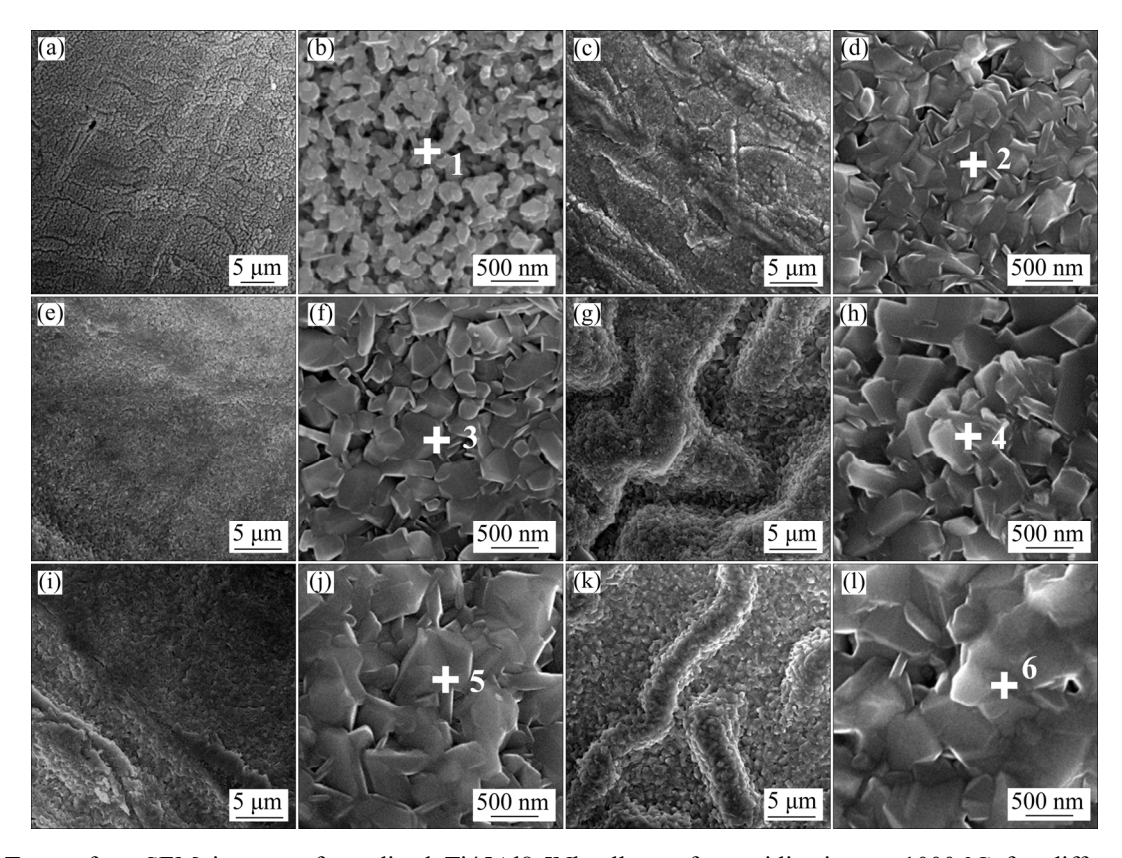


Fig. 3 Top-surface SEM images of anodized Ti45Al8.5Nb alloys after oxidization at 1000 °C for different time: (a, b) 1 h; (c, d) 5 h; (e, f) 10 h; (g, h) 20 h; (i, j) 50 h; (k, l) 100 h

Table 3 Chemical compositions of positions marked in Fig. 3

D'4'	Composition/at.%			
Position	Ti	Al	Nb	O
1	12.42	18.38	2.02	67.18
2	10.21	22.84	1.18	65.77
3	15.31	18.44	1.88	64.37
4	9.39	28.04	0.49	62.08
5	5.98	25.34	0.92	67.76
6	9.67	28.57	0.48	61.28

increases with the oxidation. This dense and Al-enriched oxide scale can effectively prevent the inward diffusion of oxygen and the outward diffusion of titanium, thereby improving the oxidation resistance of Ti45Al8.5Nb alloy.

Figure 4 shows the XRD patterns of the anodized Ti45Al8.5Nb alloys after oxidization at 1000 °C for different time. As shown in Fig. 4(a), only TiAl and Ti₃Al, the main composition of the substrate, can be detected from the anodized Ti45Al8.5Nb alloy. This is because the anodic film

is so thin that the X-ray is capable to reach the substrate (Fig. 5(a)). For the specimens oxidized from 1 to 100 h, similar characteristic peaks are observed. Specifically, besides the TiAl and Ti₃Al derived from the substrate matrix, all oxide scales are composed of TiO₂, Al₂O₃, and AlNb₂ with slightly different peak intensities. No obvious Nb-based oxides are observed probably due to the low content. A similar phenomenon is also reported by other researchers. For example, LIN et al [15] observed Nb-rich phase (AlNb₂) at the oxide scale/metal interface for the Ti45Al8.5Nb alloy oxidized at 900 °C for 100 h.

3.3 Cross-sectional morphology of anodized Ti45Al8.5Nb alloy

Figure 5 shows the cross-sectional BSE images of the anodized Ti45Al8.5Nb alloys after oxidization at 1000 °C for different time. The corresponding element distribution maps are also given. As displayed in Fig. 5(a), a thin film is observed on the anodized Ti45Al8.5Nb alloy. The EDS measurement (Points 1 and 2 in Fig. 5(a) and Table 4) and elements distribution maps (Fig. 5(b))

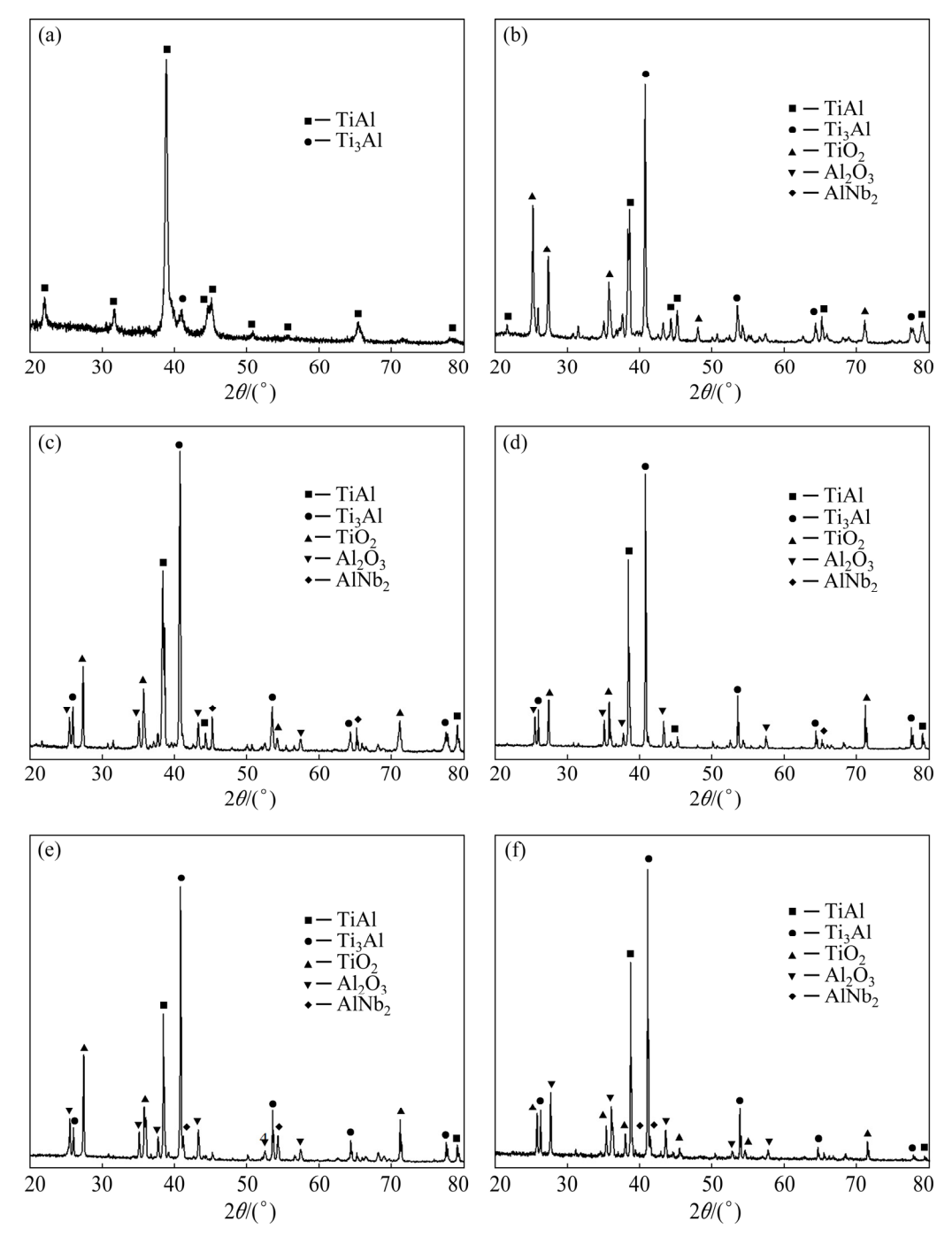


Fig. 4 XRD patterns of anodized Ti45Al8.5Nb alloys before (a) and after oxidation at 1000 °C for 1 h (b), 10 h (c), 20 h (d), 50 h (e), and 100 h (f)

indicate that the anodic film with a thickness of several hundred nanometers is fluorine-enriched.

After oxidation at 1000 °C for 10 h, an obvious oxide scale with a thickness of ${\sim}4~\mu m$ is observed on the anodized Ti45Al8.5Nb alloy (Fig. 5(c)). Combined with the XRD results (Fig. 4(c)), cross-sectional BSE image, and elements distribution maps, it can be deduced that the outmost layer of the oxide scale comprises the

mixture of (Ti, Nb)O₂ and Al₂O₃ (see Point 3 in Table 4, Figs. 5(c) and (d)). Different from TiO₂, (Ti, Nb)O₂ is compact and protective [15]. Beneath this layer, there is an Al-depleted inner layer dispersed with island-like precipitates. Based on the XRD result (Fig. 4(c)) and EDS analysis (see Point 4 in Fig. 5(c) and Table 4), it can be deduced that these precipitates are mainly composed of Al₂O₃. The generation of Al₂O₃ islands in the inner layer is

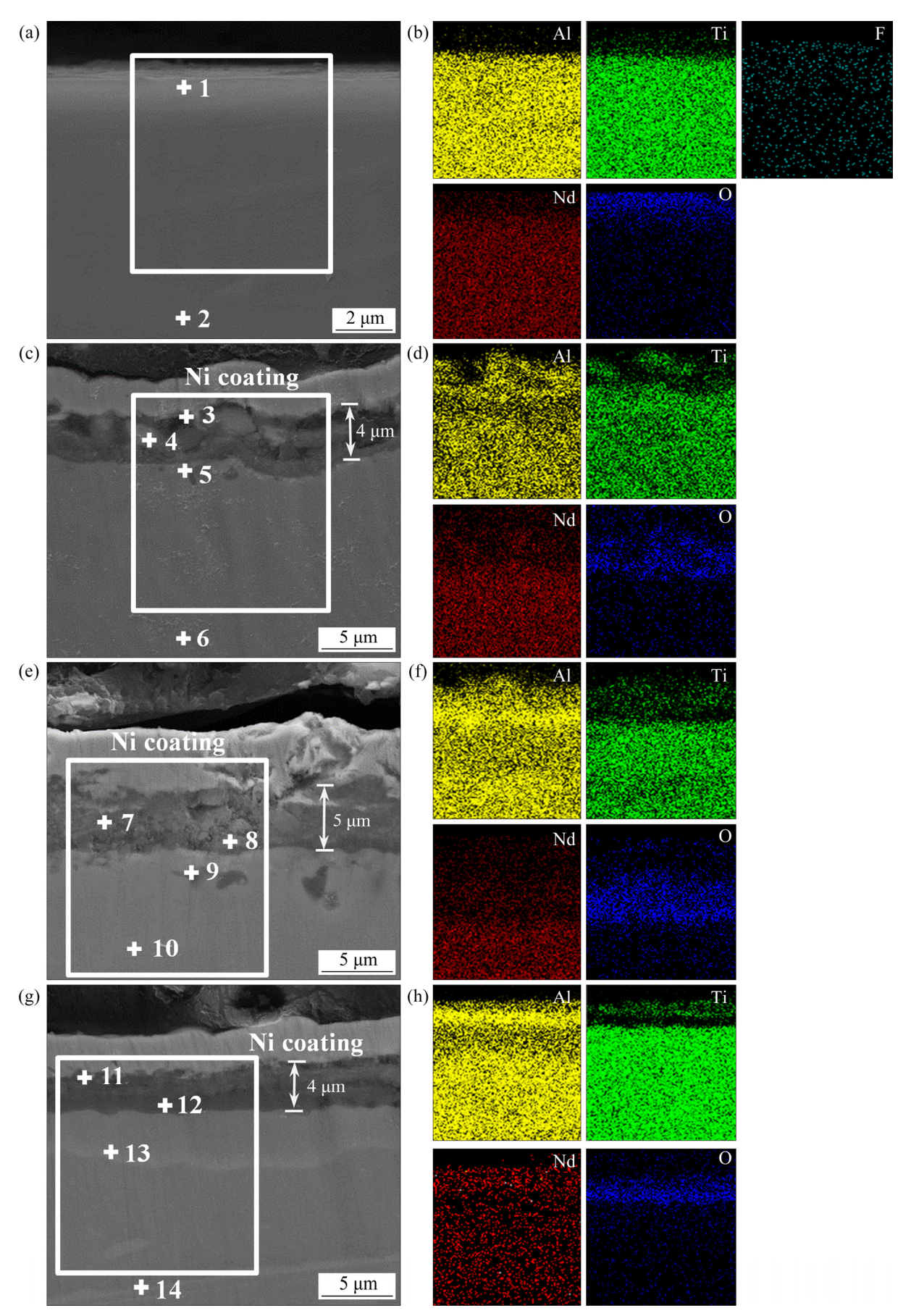


Fig. 5 Cross-sectional BSE images (a, c, e, g) and corresponding elements distribution maps (b, d, f, h) of anodized Ti45Al8.5Nb alloys before (a, b) and after oxidization at 1000 °C for 10 h (c, d), 50 h (e, f), and 100 h (g, h)

Table 4 Chemical compositions of positions marked in Fig. 5

Position	Composition/at.%				
	Ti	Al	Nb	O	F
1	32.23	28.50	4.87	32.53	1.87
2	47.11	39.34	8.81	4.74	_
3	28.18	23.68	4.16	43.98	_
4	9.47	24.93	1.47	64.13	_
5	34.91	23.3	6.41	35.38	_
6	47.03	41.45	7.31	4.21	_
7	13.38	15.95	2.11	68.56	_
8	28.97	24.89	6.57	39.57	-
9	41.54	27.65	7.90	22.91	_
10	42.08	44.55	9.29	4.08	_
11	24.88	30.98	3.76	40.38	_
12	28.57	45.54	5.75	20.14	-
13	30.88	44.98	6.04	18.10	_
14	39.95	46.28	8.67	5.10	_

directly related to the formation of the compact Al₂O₃ outmost layer, resulting in the decreased oxygen partial pressure and selective oxidation of Al in the Ti45Al8.5Nb alloy. With the prolonging of oxidation time, the thickness of the oxide scale increases to 5 µm (Fig. 5(e)). This can be attributed to the growth of Al₂O₃ islands beneath the oxide layer. Interestingly, after oxidation for 50 h, some island-like precipitates consisting of (Ti, Nb)₅Al₃O₂ are found beneath the oxide scale (see Point 9 in Fig. 5(e) and Table 4). Generally, a continuous Ti₅Al₃O₂ (Z phase) layer would generate between the oxide scale and substrate when the untreated TiAl alloy was exposed to air at high temperatures [38]. This Ti₅Al₃O₂ layer is unstable and will be decomposed into TiO₂ and Al₂O₃ [39]. Whereas, only some (Ti, Nb)₅Al₃O₂ precipitates can be found in the oxide scale generated on the anodized Ti45A8.5Nb alloy. This indicates that anodization in NH₄F-containing electrolyte can obviously improve the microstructure of the oxide scale. After oxidation for 100 h, the compact outmost layer of the oxide scale is Al₂O₃-enriched (see Points 11 and 12 in Figs. 5(g, h) and Table 4). Notably, the thickness of the oxide layer slightly decreases to $\sim 4 \mu m$ at this stage. This is because, with the prolonging time of exposure to air, the oxide layer becomes denser and denser.

3.4 Mechanical properties of anodized Ti45Al8.5Nb alloy

During the exposure to air at 1000 °C, the evolution of the mechanical properties of the anodized Ti45Al8.5Nb alloys was investigated by a nanoindentation test. As displayed in Fig. 6, the elastic modulus and hardness of the specimens possess a similar variation, and decrease firstly and then increase. This is because the elastic modulus and hardness of the specimen are highly dependent on the surface structure and composition which will change when exposed to air at high temperatures. In detail, anodization makes the elastic modulus and hardness of the Ti45Al8.5Nb alloy decrease from 86.03 GPa and 3.24 GPa to 57.16 GPa 0.94 GPa, respectively. Both the elastic modulus and hardness of the anodized Ti45Al8.5Nb alloy further decrease and reach the minimum values after oxidation for 10 h, then they increase gradually. After oxidation for 100 h, the elastic modulus and hardness of the anodized Ti45Al8.5Nb alloy are 92.3 and 6.72 GPa, respectively. This is because with the prolonging of the oxidation time the anodized Ti45Al8.5Nb alloy with pores and micro-cracks structure is gradually covered by continuous and dense protective Al₂O₃ which has high hardness.

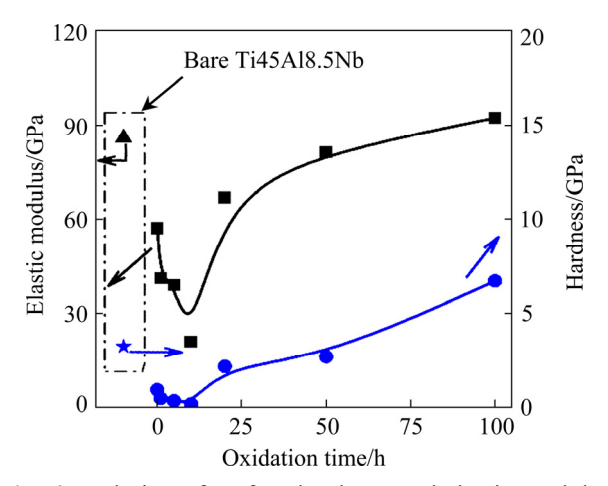


Fig. 6 Evolution of surface hardness and elastic modulus of anodized Ti45Al8.5Nb alloys after oxidation at 1000 °C for different time

3.5 Friction coefficient and wear behavior of anodized Ti45Al8.5Nb alloy

The friction coefficient and wear behavior of bare and anodized Ti45Al8.5Nb alloys after oxidation for different time were characterized using Al_2O_3 balls as the counterpart. Figure 7 shows

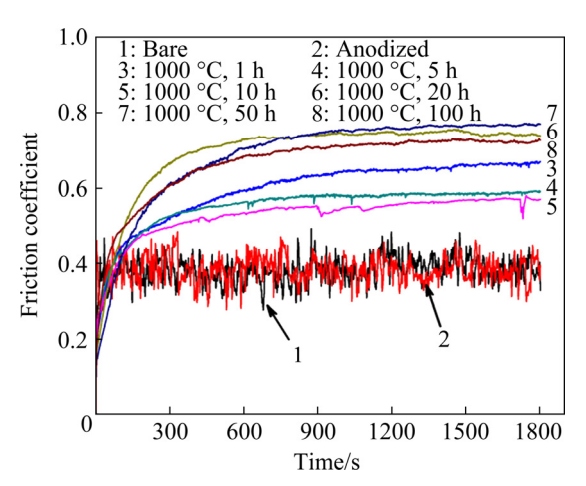


Fig. 7 Friction coefficients of bare (1) and anodized (2–8) Ti45Al8.5Nb alloys after oxidization at 1000 °C for different time

the friction coefficients of the specimens as a function of dry sliding time. The bare (Curve 1) and pristine anodized (Curve 2) Ti45Al8.5Nb alloys possess similar friction coefficients which are fluctuant during the whole test. After exposure to air at 1000 °C, a spontaneous increase in the friction coefficient can be found for all specimens (Curves 3–8). This is because during the initial stage of the wear test, the outmost layer is easy to be damaged, resulting in the generation of loose wear debris with small size. These particles have little influence on the ploughing friction, leading to a small friction coefficient. Whereas, at the end of this stage (after wear test for 100-300 s), the accumulation and entrapment of large wear particles result in ploughing friction and a rapid increase in the friction coefficient. Interestingly, after oxidation at 1000 °C for different time, all the friction coefficients of the anodized Ti45Al8.5Nb alloys are higher than those of the bare and pristine anodized specimens. It is known that the wear resistance of a material is the combination of strength/hardness and ductility [40,41]. As reported, the yielding strength decreases but tensile plasticity increases when the Ti45Al8.5Nb alloy is serviced under high temperatures [42]. On the other hand, the oxidation of the fluorine-enriched anodic film results in the generation of Al₂O₃ whose content increases with the prolonging of oxidation (Fig. 4). WU et al [43] investigated the influence of microarc oxidation on the wear resistance of the TiAl alloy. Results show that the friction coefficient of the micro-arc oxidation coating consisting of Al₂TiO₅, Al₂SiO₅, and TiO₂ is much higher than that of the untreated TiAl substrate. YAN et al [44] also reported that the friction coefficient of the micro-arc oxidation treated Al alloy was higher than that of the untreated Al alloy. The variation of the friction coefficient and mechanical properties of the specimens are attributed to the evolution of the surface morphology and chemical composition of the oxide scale. As shown in Fig. 5, when exposed to air at high temperatures the oxide scale on the anodized alloy changes from loose to dense structure, which is consistent with the trend of the friction coefficient and mechanical properties.

After the friction wear test, the morphologies of the wear tracks were characterized by SEM. Generally, the wear resistance of a sample is highly dependent on the surface hardness. The wear track morphology indicates that abrasive wear is the dominant wear process for bare Ti45Al8.5Nb alloy (Fig. 8(a)). And the image taken from the edge of the wear track reveals that the depth of the track is $\sim 20 \mu m$ (Fig. 8(b)). This is because compared with the Al₂O₃ counterpart ball, the hardness of the Ti45Al8.5Nb matrix is lower and more prone to deform plastically. For the anodized Ti45Al8.5Nb alloy, more fragments are observed in the wear track whose depth is similar to that of bare Ti45Al8.5Nb alloy (Figs. 8(c) and (d)). This result is well consistent with the nanoindentation test, which reveals that the hardness of the anodized alloy is lower than that of the bare alloy (Fig. 6). Whereas, wear tracks with different characteristics are observed when the anodized Ti45Al8.5Nb alloys are exposed to air at 1000 °C. As shown in Figs. 8(e-h), with the prolonging of exposure time the width of the wear tracks is gradually reduced and fewer fragments can be found in the wear tracks. This is attributed to the generation of glazed oxides scale whose composition is changed with the oxidation time. Oxidation for 10 h leads to the formation of the Al₂O₃-based oxide scale, which increases the coefficient of friction and decreases the wear loss.

The profiles of the wear tracks of bare and anodized Ti45Al8.5Nb alloys after oxidation for different time are displayed in Fig. 9. From the perspective of the 2D profile, the wear depth of the bare Ti45Al8.5Nb alloy is quite deep and reaches $18 \, \mu m$. This is because the Al_2O_3 ball has higher hardness than the Ti45Al8.5Nb alloy and the

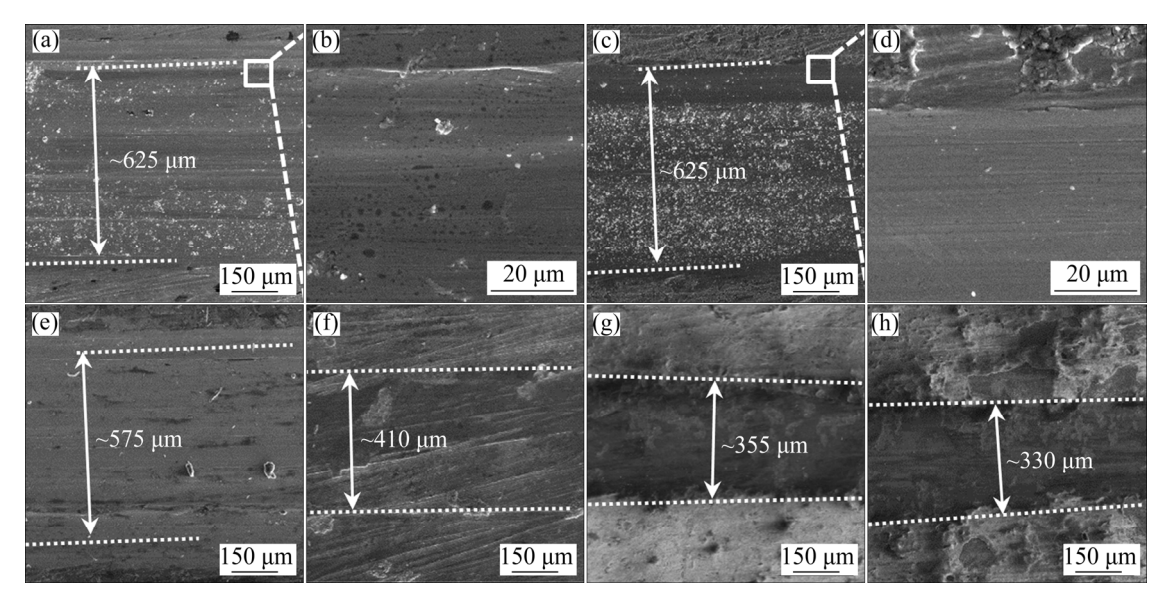


Fig. 8 Top-surface SEM images of wear tracks of bare (a, b) and pristine anodized (c, d) Ti45Al8.5Nb alloys, and anodized Ti45Al8.5Nb alloys after oxidization at 1000 °C for 1 h (e), 10 h (f), 50 h (g) and 100 h (h) ((b) and (d) are the enlarged images taken at the edge of the wear tracks)

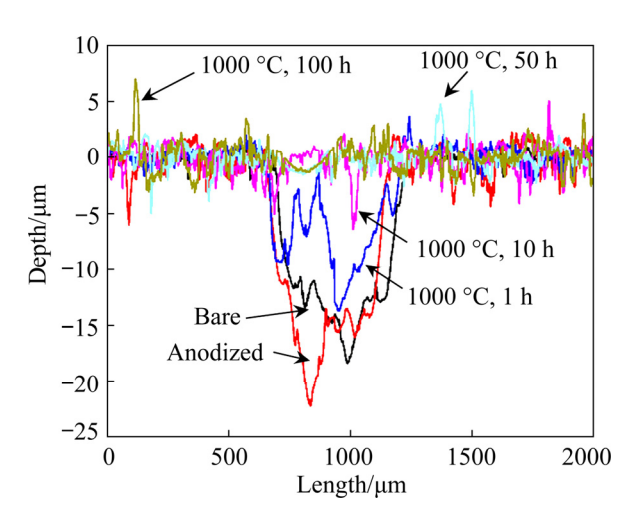


Fig. 9 Profiles of wear tracks of bare and anodized Ti45Al8.5Nb alloys after oxidation at 1000 °C for different time

abrasive wear is dominated during the wear process. Whereas, the wear depth of the pristine anodized Ti45Al8.5Nb alloy is slightly increased to 22 μm . This is attributed to the porous and discontinuous anodic film is easy to be removed by the counterpart ball, resulting in a deep scratch. Such wear behavior is weakened by the formation of Al₂O₃-based oxide scale when the anodized Ti45Al8.5Nb alloy is exposed to air at 1000 °C. After oxidation for 100 h, the wear depth of the specimen is dramatically reduced to $\sim\!\!2~\mu m$. The lowest wear depth and narrowest wear width of the

anodized Ti45Al8.5Nb alloy manifest that anodization is beneficial to improving the anti-friction and anti-wear properties.

Figure 10 illustrates the variations of the wear loss of bare and anodized Ti45Al8.5Nb alloys. The wear loss of the specimens in the friction wear test can be calculated according to

$$V=LdH$$
 (1)

where V, L, d, and H are the wear loss, wear length, wear width, and mean maximum wear depth, respectively.

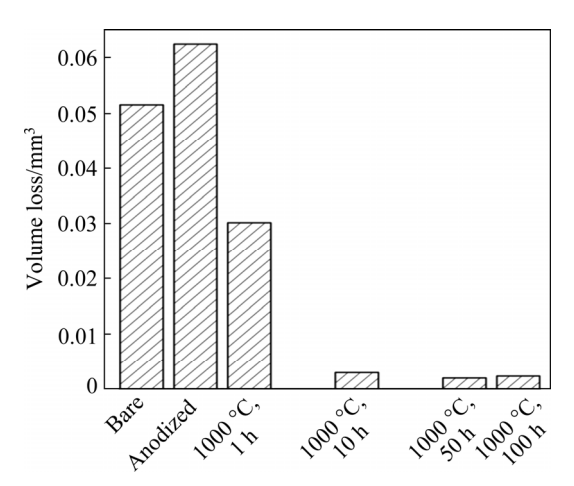


Fig. 10 Wear volume loss obtained from wear track of bare and pristine anodized Ti45Al8.5Nb alloys, and anodized Ti45Al8.5Nb alloys after oxidation at 1000 °C for different time

It is shown that the wear loss increases from 0.052 mm³ for bare Ti45Al8.5Nb alloy to 0.062 mm³ for the pristine anodized alloy. This is consistent with the SEM results (Figs. 8(a-d)) and profiles of the wear tracks (Fig. 9). The anodic film composed of segregated particles is easy to be destroyed by the counterpart Al₂O₃ ball, resulting in increased wear loss. When exposed to air at high temperatures, the wear resistance of the anodized Ti45Al8.5Nb alloy is dramatically improved. In detail, after oxidation for 100 h, the wear loss of the anodized alloy significantly decreases to 0.0023 mm³, which is only 4.5% to that of the bare Ti45Al8.5Nb alloy. This decline is ascribed to the change in the morphology and composition of the oxide scale whose outmost layer is composed of compact and contiguous Al₂O₃ matrix.

4 Conclusions

- (1) When exposured to air at high temperatures, the fluorine- and aluminum-enriched anodic film was oxidized into a compact Al₂O₃ layer, which could provide excellent oxidation performance and good wear resistance.
- (2) After oxidation for 100 h, the mass gain of the anodized Ti45Al8.5Nb alloy was 0.37 mg/cm², which was less than 10% of the untreated specimen.
- (3) The tribological properties of the anodized Ti45Al8.5Nb alloy were greatly associated with the morphology and composition of the oxide scale. With the prolonging of oxidation time, the hardness and elastic modulus of the anodized Ti45Al8.5Nb alloy were increased obviously. Meanwhile, the anti-friction and anti-wear properties were also significantly improved.

Acknowledgments

The authors are grateful for the financial supports from the National Natural Science Foundation of China (No. 51971205), the Guangdong Basic and Applied Basic Research Foundation, China (No. 2021B1515020056), and the Shenzhen Fundamental Research Program, China (No. JCYJ20190807154005593).

References

[1] PFLUMM R, FRIEDLE S, SCHUETZE M. Oxidation protection of γ -TiAl-based alloys—A review [J].

- Intermetallics, 2015, 56: 1-14.
- [2] DAI Jing-jie, ZHU Ji-yun, CHEN Chuan-zhong, WENG Fei. High temperature oxidation behavior and research status of modifications on improving high temperature oxidation resistance of titanium alloys and titanium aluminides: A review [J]. Journal of Alloys and Compounds, 2016, 685: 784–798.
- [3] GARIP Y, OZDEMIR O. Comparative study of the oxidation and hot corrosion behaviors of TiAl-Cr intermetallic alloy produced by electric current activated sintering [J]. Journal of Alloys and Compounds, 2019, 780: 364–377.
- [4] GARIP Y, OZDEMIR O. Corrosion behavior of the resistance sintered TiAl based intermetallics induced by two different molten salt mixture [J]. Corrosion Science, 2020, 174: 108819.
- [5] SHAABAN A, HAYASHI S, TAKEYAMA M. A comparative study on the oxidation behaviours of a TNM alloy in argon and oxygen atmospheres at 650 °C [J]. Corrosion Science, 2021, 185: 109415.
- [6] KIM S W, HONG J K, NA Y S, YEOM J T, KIM S E. Development of TiAl alloys with excellent mechanical properties and oxidation resistance [J]. Materials & Design, 2014, 54: 814–819.
- [7] KHAN A, HUANG Yuan-chao, DONG Zhi-hong, PENG Xiao. Effect of Cr₂O₃ nanoparticle dispersions on oxidation kinetics and phase transformation of thermally grown alumina on a nickel aluminide coating [J]. Corrosion Science, 2019, 150: 91–99.
- [8] LI Yan-feng, XU Hui, SONG Zhao-quan, MA Song-shan. Effect of Nb on plasticity and oxidation behavior of TiAlNb intermetallic compound by density functional theory [J]. Journal of Central South University of Technology, 2010, 17(4): 674–682.
- [9] JIANG Hui-ren, HIROHASI M, LU Yun, IMANARI H. Effect of Nb on the high temperature oxidation of Ti– (0–50 at.%)Al [J]. Scripta Materialia, 2002, 46(9): 639–643.
- [10] LI Min-gao, XIAO Shu-long, CHEN Yu-yong, XU Li-juan, TIAN Jing. The effect of boron addition on the high-temperature properties and microstructure evolution of high Nb containing TiAl alloys [J]. Materials Science and Engineering A, 2018, 733: 190–198.
- [11] DONG Zi-qiang, JIANG Hui-ren, FENG Xiao-ran, WANG Zhong-lei. Effect of Cr on high temperature oxidation of TiAl [J]. Transactions of Nonferrous Metals Society of China, 2006, 16(S3): s2004–s2008.
- [12] PAN Yu, LU Xin, HUI Tai-long, LIU Cheng-cheng, LIU Bo-wen, XU Wei, ZHANG Ce, SUN Jian-zhuo, QU Xuan-hui, ZHANG Jia-zhen. High-temperature oxidation behaviour of TiAl alloys with Co addition [J]. Journal of Materials Science, 2021, 56(1): 1–13.
- [13] WU Ya-dian, HAGIHARA K, UMAKOSHI Y. Influence of Y-addition on the oxidation behavior of Al-rich γ-TiAl alloys [J]. Intermetallics, 2004, 12(5): 519–532.
- [14] JIANG Hui-ren, WANG Zhong-lei, MA Wen-shuai, FENG Xiao-ran, DONG Zi-qiang, ZHANG Liang, LIU Yong. Effects of Nb and Si on high temperature oxidation of TiAl [J]. Transactions of Nonferrous Metals Society of China, 2008, 18(3): 512–517.

- [15] LIN Jun-pin, ZHAO Li-li, LI Guan-yuan, ZHANG Lai-qi, SONG Xi-ping, YE Feng, CHEN Guo-liang. Effect of Nb on oxidation behavior of high Nb containing TiAl alloys [J]. Intermetallics, 2011, 19(2): 131–136.
- [16] ZSCHAU H E, ZHAO W, NEVE S, GLEESON B, SCHUETZE M. Promotion of the Al₂O₃-scale formation on Ni-Cr-Al alloys via the fluorine effect [J]. Oxidation of Metals, 2015, 83(3): 335-349.
- [17] SCHÜTZE M. The role of surface protection for high-temperature performance of TiAl alloys [J]. JOM, 2017, 69(12): 2602–2609.
- [18] DONCHEV A, RICHTER E, SCHÜTZE M, YANKOV R. Improving the oxidation resistance of TiAl-alloys with fluorine [J]. Journal of Alloys and Compounds, 2008, 452(1): 7–10.
- [19] DONCHEV A, SCHÜTZE M, STRÖM E, GALETZ M. Oxidation behaviour of the MAX-phases Ti₂AlC and (Ti,Nb)₂AlC at elevated temperatures with and without fluorine treatment [J]. Journal of the European Ceramic Society, 2019, 39(15): 4595–4601.
- [20] WANG Ji-qiang, KONG Ling-yan, LI Tie-fan, XIONG Tian-ying. High temperature oxidation behavior of Ti(Al,Si)₃ diffusion coating on γ-TiAl by cold spray [J]. Transactions of Nonferrous Metals Society of China, 2016, 26(4): 1155–1162.
- [21] ZHANG Kai, XIN Li, LU Yi-liang, CHENG Yu-xian, WANG Xiao-lan, ZHU Sheng-long, WANG Fu-hui. Improving oxidation resistance of γ-TiAl based alloy by depositing TiAlSiN coating: Effects of silicon [J]. Corrosion Science, 2021, 179: 109151.
- [22] JIANG Zhi-peng, YANG Xu, LIANG Yong-feng, HAO Guo-jian, ZHANG Hui, LIN Jun-pin. Favorable deposition of gamma-Al₂O₃ coatings by cathode plasma electrolysis for high-temperature application of Ti-45Al-8.5Nb alloys [J]. Surface and Coatings Technology, 2017, 333: 187–194.
- [23] YANG Xu, JIANG Zhi-peng, HAO Guo-jian, LIANG Yong-feng, DING Xian-fei, LIN Jun-pin. Ni-doped Al₂O₃ coatings prepared by cathode plasma electrolysis deposition on Ti-45Al-8.5 Nb alloys [J]. Applied Surface Science, 2018, 455: 144-152.
- [24] WANG Shao-qing, XIE Fa-qin, WU Xiang-qing, MA Yong, DU Hao-xuan, WU Gang. Cathodic plasma electrolytic deposition of ZrO₂/YSZ doped Al₂O₃ ceramic coating on TiAl alloy [J]. Ceramics International, 2019, 45(15): 18899–18907.
- [25] RASTKAR A R, BLOYCE A, BELL T. Sliding wear behaviour of two gamma-based titanium aluminides [J]. Wear, 2000, 240(1): 19–26.
- [26] CHENG Jun, YANG Jun, ZHANG Xing-hua, ZHONG Hong, MA Ji-qiang, LI Fei, FU Li-cai, BI Qin-ling, LI Jin-shan, LIU Wei-min. High temperature tribological behavior of a Ti-46Al-2Cr-2Nb intermetallics [J]. Intermetallics, 2012, 31: 120-126.
- [27] QIU Jing-wen, LIU Yong, MENG Fan-ling, BAKER I, MUNROE P R. Effects of environment on dry sliding wear of powder metallurgical Ti-47Al-2Cr-2Nb-0.2W [J]. Intermetallics, 2014, 53: 10-19.
- [28] LIU Zhan-qi, MA Rui-xin, XU Guo-jian, WANG Wen-bo, SU Yun-hai. Effects of annealing on microstructure and

- mechanical properties of γ -TiAl alloy fabricated via laser melting deposition [J]. Transactions of Nonferrous Metals Society of China, 2020, 30(4): 917–927.
- [29] LI Xi-jin, CHENG Guo-an, XUE Wen-bin, ZHENG Rui-ting, CHENG Yun-jun. Wear and corrosion resistant coatings formed by microarc oxidation on TiAl alloy [J]. Materials Chemistry and Physics, 2008, 107(1): 148–152.
- [30] WANG Fang, MIAO Qiang, LIANG Wen-ping, REN Bei-lei, PEI Qiu-xu. Effect of heat treatment on tribological properties of TA15 titanium alloy [J]. Journal of Materials Heat Treatment, 2015, 36(S1): 91–95.
- [31] TIAN Su-gui, LV Xiao-xia, YU Hui-chen, WANG Qi, JIAO Ze-hui, SUN Hao-fang. Creep behavior and deformation feature of TiAl–Nb alloy with various states at high temperature [J]. Materials Science and Engineering A, 2016, 651: 490–498.
- [32] XU Yi, MIAO Qiang, LIANG Wen-ping, YU Xiu-shui, JIANG Qiong, ZHANG Zhi-gang, REN Bei-lei, YAO Zheng-jun. Tribological behavior of Al₂O₃/Al composite coating on γ-TiAl at elevated temperature [J]. Materials Characterization, 2015, 101: 122–129.
- [33] MO Min-hua, WU Lian-kui, CAO Hua-zhen, LIN Jun-pin, ZHENG Guo-qu. Halogen effect for improving high temperature oxidation resistance of Ti-50Al by anodization [J]. Applied Surface Science, 2017, 407: 246-254.
- [34] WU Lian-kui, XIA Jun-jie, JIANG Mei-yan, WANG Qi, WU Hai-xin, SUN Dong-bai, YU Hong-ying, CAO Fa-he. Oxidation behavior of Ti45Al8.5Nb alloy anodized in NH₄F containing solution [J]. Corrosion Science, 2020, 166: 108447.
- [35] MO Min-hua, WU Lian-kui, CAO Hua-zhen, LIN Jun-pin, LU Dong-hui, ZHENG Guo-qu, High temperature oxidation behavior and anti-oxidation mechanism of Ti-50Al anodized in ionic liquid [J]. Surface and Coatings Technology, 2016, 307: 190-199.
- [36] XIA Jun-jie, NIU Hong-zhi, LIU Min, CAO Hua-zhen, ZHENG Guo-qu, WU Lian-kui. Enhancement of high temperature oxidation resistance of Ti48Al5Nb alloy via anodic anodization in NH₄F containing ethylene glycol [J]. Journal of Chinese Society for Corrosion and Protection, 2019, 39(2): 96–105.
- [37] SU Yu, KONG Fan-tao, WANG Zhen-bo, WANG Xiao-peng, CHEN Yu-yong. Oriented porous anodic oxide layers on Ti-50Al with outstanding oxidation resistance at 800 °C [J]. Corrosion Science, 2019, 159: 108146.
- [38] WU Lian-kui, WU Wei-yao, SONG Jia-lin, HOU Guang-ya, CAO Hua-zhen, TANG Yi-ping, ZHENG Guo-qu. Enhanced high temperature oxidation resistance for γ-TiAl alloy with electrodeposited SiO₂ film [J]. Corrosion Science, 2018, 140: 388–401.
- [39] COPLAND E H, GLEESON B, YOUNG D J. Formation of Z-Ti₅₀Al₃₀O₂₀ in the sub-oxide zones of γ-TiAl-based alloys during oxidation at 1000 °C [J]. Acta Materialia, 1999, 47(10): 2937–2949.
- [40] MENGIS L, GRIMME C, GALETZ M C. High-temperature sliding wear behavior of an intermetallic γ -based TiAl alloy [J]. Wear, 2019, 426–427: 341–347.
- [41] XU Xiang-jun, LIN Jun-pin, GUO Jian, LIANG Yong-feng. Friction weldability of a high Nb containing TiAl alloy [J].

- Materials, 2019, 12(21): 3556.
- [42] CHENG Fang, LIN Jun-pin, LIANG Yong-feng. Friction and wear properties of a high Nb-containing TiAl alloy against WC-8Co, Si₃N₄, and GCr₁₅ in an unlubricated contact [J]. Intermetallics, 2019, 106: 7–12.
- [43] WU Xiang-qing, XIE Fa-qin, HU Zong-chun, WANG Li. Effects of additives on corrosion and wear resistance of micro-arc oxidation coatings on TiAl alloy [J]. Transactions
- of Nonferrous Metals Society of China, 2010, 20(6): 1032–1036.
- [44] YAN Han, WANG Jian-cheng, MENG Cai, WANG Xun, SONG Shi-jie, FAN Xiao-qiang, ZHANG Lin, LI Hao, LI Wen, ZHU Min-hao. Towards long-term corrosion and wear protection of Al alloy: Synergy of Ti₃C₂T_x flake and micro-arc oxidation coating [J]. Corrosion Science, 2020, 174: 108813.

阳极氧化 Ti45Al8.5Nb 合金的高温氧化及摩擦学性能

李哲轩1,包雅婷2,伍廉奎1,曹发和1

1. 中山大学·深圳 材料学院 518107;

2. 浙江工业大学 材料科学与工程学院, 杭州 310014

摘 要:采用阳极氧化技术在含 0.15 mol/L NH₄F 的乙二醇中对 Ti45Al8.5Nb 合金进行阳极氧化处理。研究阳极氧化 Ti45Al8.5Nb 合金的高温氧化性能和摩擦学行为。结果表明,由于保护性氧化层的产生,经阳极氧化处理的 Ti45Al8.5Nb 合金表现出良好的抗高温氧化性能。经 $1000\,^{\circ}$ C 氧化 $100\,h$ 后,阳极氧化 Ti45Al8.5Nb 合金的增重仅为 $0.37\,$ mg/cm²。另一方面,阳极氧化 Ti45Al8.5Nb 合金的硬度和弹性模量随高温氧化时间的延长先降低后升高,主要原因是富 Al_2O_3 的最外层氧化层的生成。

关键词: TiAl 合金; 阳极氧化; 高温氧化; 摩擦学性能

(Edited by Xiang-qun LI)